Molecular Therapy
Oncology
Original Article

Newcastle disease virus harboring the PTEN gene inhibits pancreatic cancer growth by inhibiting PI3K/AKT/mTOR signaling and activating apoptosis

Seonhee Kim,[1] Bo-Kyoung Jung,[1] Jinju Kim,[1] Joo Hee Jeon,[1] Sung Hoon Jang,[2] Minsoo Kim,[3] Cuk-Seong Kim,[3] and Hyun Jang[1]

[1]Libentech Co. Ltd., Daejeon 34013, Republic of Korea; [2]Graduate School of Medical Science and Engineering, Korea Advanced Institute of Science and Technology (KAIST), Daejeon 34141, Republic of Korea; [3]Department of Physiology & Medical Science, College of Medicine, Chungnam National University, Daejeon 35015, Republic of Korea

Pancreatic ductal adenocarcinoma (PDAC) is a highly aggressive and intractable cancer that requires more effective therapies that can improve early detection, enhance treatment efficacy, and provide better patient outcomes. Kirsten rat sarcoma viral oncogene homolog (KRAS) mutations and reduced phosphatase and tensin homolog (PTEN) protein expression are key factors driving the proliferation and severity of PDAC. To address this, a recombinant Newcastle disease virus (rNDV) containing the PTEN gene (rNDV-PTEN) was created to investigate its PDAC cell-killing and tumor-suppression effects in PDAC cells transplanted into mice. PTEN expression induced by rNDV-PTEN virus infection in KRAS-mutated PDAC cells lowered phosphatidylinositol 3-kinases (PI3K)/protein kinase B (AKT)/mammalian target of rapamycin (mTOR) signaling, promoted PDAC cell death, and suppressed tumor growth. PTEN overexpression promotes apoptotic signaling pathways in both PANC-1 cells and orthotopic xenograft mice. Additionally, during virotherapy, rNDV-PTEN-injected mice exhibited a mild immune response and no abnormal responses in blood parameters such as glucose, triglyceride, and total cholesterol levels. These findings support the potential of rNDV-PTEN as a safe and effective therapy for PDAC with highly activated PI3K/AKT/mTOR signaling caused by KRAS and PTEN gene mutations. Thus, PTEN gene-containing rNDV may be a promising candidate for pancreatic cancer treatment.

INTRODUCTION

Pancreatic ductal adenocarcinoma (PDAC) is one of the most serious and aggressive forms of cancer, with an average 5-year survival rate of less than 10%.[1] PDAC originates from the cells lining the pancreatic ducts and accounts for the majority of pancreatic cancer cases. Early prognosis of PDAC is difficult due to the deep-seated location of the pancreas and the absence of specific symptoms in the early stages of the disease. The aggressive behavior of PDAC, with rapid growth and high metastatic propensity, makes its control difficult even with aggressive treatment approaches.[2] Noninvasive diagnostic methods have not yet been established because there are no reliable early-stage biomarkers. For these reasons, most patients are not diagnosed at an early stage, do not receive surgical treatment, and depend only on chemical treatment.[3] Although chemotherapy and radiation therapy may reduce disease severity and help manage symptoms, they do not provide a cure. Therefore, development of more advanced and effective therapeutics and methods for early diagnosis are critical for improving the prognosis of patients with pancreatic cancer.

Genetic investigations of numerous tumors have led to the discovery of closely linked genes implicated in cancer occurrence and progression.[4] Several oncogenes and tumor-suppressor genes have been identified and their genetic alterations are known to be a major cause of cancer.

Kirsten rat sarcoma viral oncogene homolog (KRAS) mutations are observed in more than 90% of patients with PDAC. These mutations activate the phosphatidylinositol 3-kinases (PI3K)/protein kinase B (AKT)/mammalian target of rapamycin (mTOR) signaling pathway, promoting cancer cell growth and activating metastasis and angiogenesis.[5] The activation of the PI3K/AKT/mTOR signaling pathway promotes cell survival and proliferation by inhibiting apoptosis and promoting cell cycle progression. Additionally, activated AKT modulates other signaling pathways, contributing to the aggressive nature of cancer cells.[6]

The phosphatase and tensin homolog (PTEN) protein plays crucial roles in the development of cancer. Loss or reduced expression of this protein can lead to the dysregulation of critical cellular processes, promoting tumor growth, metastasis, and resistance to treatment.[7] Canonical PTEN encodes a 403-amino acid peptide composed of five structural-functional domains: an N-terminal phosphatidylinositol

Received 14 February 2024; accepted 24 October 2024;
https://doi.org/10.1016/j.omton.2024.200898.

Correspondence: Hyun Jang, Libentech Co. Ltd., Daejeon 34013, Republic of Korea.
E-mail: vacchyun@libentech.kr

4,5-bisphosphate (PIP2)-binding domain with phosphatase activity responsible for dephosphorylation of phospholipids, a C2 domain for membrane targeting, a regulatory C-terminal tail with multiple phosphorylation sites (Ser362, Thr366, Ser370, Ser380, Ser382, Thr382, Thr383, and Ser385), a PEST sequence (Pro, Glu, Ser, and Thr), and aPDZ (PSD-95, Dlg1, and ZO-1) domain-binding motif involved in the regulation of PTEN activity and stability.[8]

The phosphatase function of PTEN helps regulate the PI3K/AKT/mTOR pathway, which is involved in cell proliferation, survival, and metabolism.[9] PTEN dephosphorylates phosphatidylinositol[3–5]-trisphosphate (PIP3) to produce PIP_2, resulting in the inhibition of the AKT signaling pathway.[10] Loss of PTEN function, through genetic mutations, deletions, or reduced protein expression, can lead to increased activation of the PI3K/AKT/mTOR pathway and uncontrolled cell growth, thereby increasing the risk of cancer development.[11] Analysis of samples from 41 patients with pancreatic cancer showed that PTEN levels are closely related to proliferation, infiltration, and metastasis in human pancreatic cancer.[12]

Loss of PTEN occurs through various mechanisms, and, in specific cancers, it is not caused by genetic alterations.[13] PTEN is not mutated in pancreatic cancers; however, lowering its expression may lead to the occurrence and progression of pancreatic cancer.[14] Several studies are currently underway to investigate the reasons underlying low PTEN levels in pancreatic cancer cells in the absence of mutations or deletions. Wenzhe et al. showed that the interaction of metastasis-associated protein 2 core subunit with the PTEN gene promoter lowered PTEN expression and led to activated proliferation, migration, and invasion of pancreatic cancer cells.[15] Ebert et al. demonstrated that transcription and translation of PTEN are regulated by transforming growth factor β 1 (TGF-β1). They showed that PTEN mRNA levels were significantly decreased in PANC-1 cells treated with TGF-β1, and PTEN expression significantly decreased in the pancreas of TGF-β1 transgenic mice. These results also showed that PTEN loss without mutations increased the proliferation and migration of pancreatic cancer cells.[14] Jiachi et al. showed that PTEN suppression in pancreatic cancer cells activated invasion and proliferation of the cells through the PI3K/AKT signaling pathway.[16] They also showed that small interfering RNA (siRNA)-mediated inhibition of PTEN gene expression increased VEGF secretion and promoted angiogenesis.[17] Nimesulide, a selective COX-2 inhibitor, enhanced PTEN expression and inhibited the proliferation of PANC-1 cells.[17] Haoqiang et al. demonstrated that KRAS mutation and PTEN deletion promoted the activity of nuclear factor κB (NF-κB), resulting in stromal activation and immune cell infiltration through the activation of the cytokine network, which are characteristics of tumor-promoting properties.[18] Recently, several studies have revealed that PTEN protein expression inhibits PI3K/AKT/mTOR signaling and induces intestinal cancer cell death.[19]

Oncolytic viruses that harbor tumor-suppressive genes, based on the genetic analysis of cancer cells, represent a new class of cancer therapies that have the advantages of selective replication in tumor cells and the delivery of tumor-suppressor genes or immune-stimulating genes leading to cancer cell death.[20] Various strains of viruses, including adenoviruses, herpesviruses, poxviruses, vaccinia viruses, and animal infectious viruses, have been engineered to possess oncolytic properties and have been studied for their potential in cancer treatment.[21] Newcastle disease virus (NDV), as an intrinsic oncolytic virus, exhibits cancer-cell-specific replication in the cytoplasm, distinguishing between cancer and normal cells without the need for genetic modification.[22,23] The highly pathogenic NDV has a strong oncolytic effect, but it can pose a serious threat as an infectious disease agent in birds such as chickens.[24] Nevertheless, the virus not only has an intrinsic oncolytic effect but also has the ability to induce cancer cell death by transferring foreign genes to cancer cells and inducing an immune response in cancer cells, resulting in various cancer-suppressing effects.[25] Upregulation or overexpression of PTEN, achieved through a recombinant oncolytic virus or plasmid DNA vector, effectively suppresses tumor cell growth and induces apoptosis in various cancers, including PDAC.[26] In a previous study, we investigated the therapeutic efficacy of recombinant NDV (rNDV) and rNDV harboring the PTEN gene (rNDV-PTEN) in xenograft mice transplanted with human brain tumor cells (T98G). rNDV-PTEN exhibited a more effective cancer cell-killing and tumor-suppressive effect than rNDV.

In this study, we evaluated the cancer cell-killing and growth-inhibitory effects of PTEN overexpression by infecting PDAC cells with an rNDV, rNDV-PTEN, using *in vitro* and PDAC cell-transplanted animal models. We also investigated the mechanisms underlying the cancer cell-killing and tumor-suppressive effects of PTEN overexpression and examined the immune and metabolic responses to rNDV-PTEN to assess its safety.

RESULTS

mRNA expression profiling and change analysis

Genetic information plays a crucial role in cancer research and drug development. We aimed to investigate mRNA alterations in pancreatic cancer tissue compared to normal tissue samples obtained from pancreatic cancer patients. The mRNA microarray expression data have been deposited in the National Center for Biotechnology Information's (NCBI) Gene Expression Omnibus (GEO: GSE183795) using the read count data of 22,465 genes from 131 pancreatic tumor tissues, 102 adjacent non-tumor tissues and three normal pancreatic tissues in humans. A multi-dimensional scaling (MDS) plot using the R package edgeR[3,27] confirmed the absence of batch effect in the RNA sequencing data from 236 samples that had been re-sequenced owing to high rRNA contamination (Figure S1A). We generated a volcano plot (a type of scatterplot) using an R package edgeR,[3] which showed the obtained fold changes and *p* values (Figure S1B). These plots show statistical significance (*p* value) versus magnitude of change (fold change) after differentially expressed gene analysis. The most upregulated genes are higher, while the most downregulated genes are toward the bottom. A false discovery rate (FDR) threshold of <0.05 was applied to identify the significant change genes. We confirmed that PTEN expression was the third most reduced gene out of

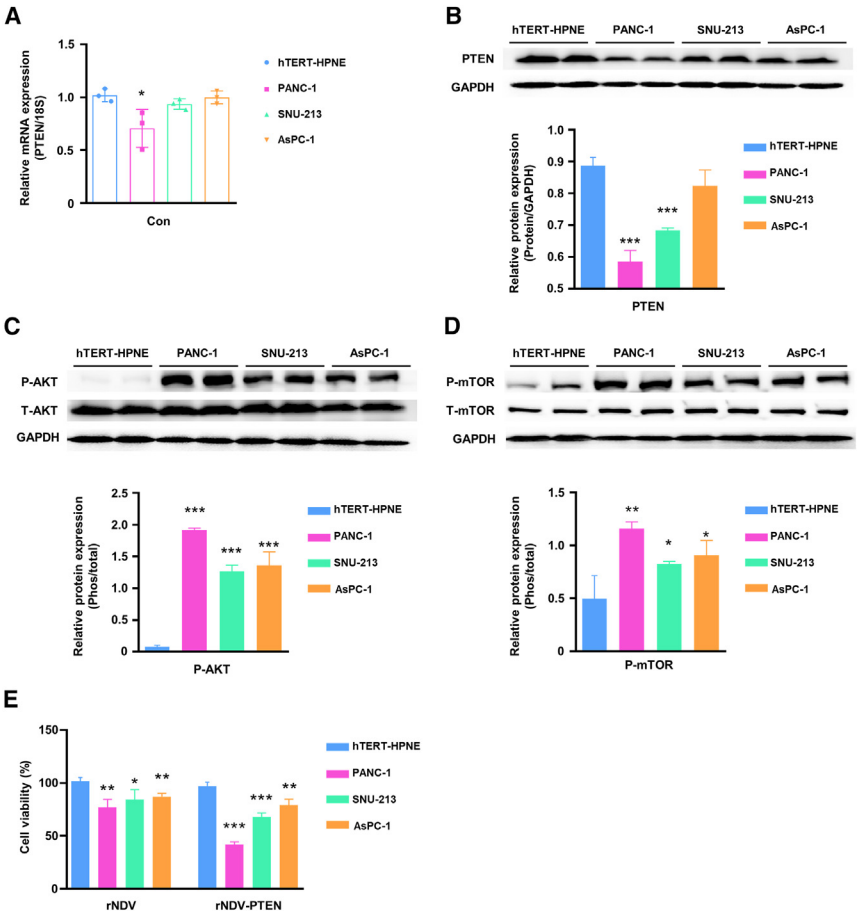

Figure 1. PTEN mRNA and PTEN, P-AKT, and P-mTOR protein levels in normal and PDAC cell lines

(A) PTEN mRNA and (B) PTEN, (C) P-AKT, and (D) P-mTOR protein levels in human normal pancreatic (hTERT-HPNE) and PDAC cell lines (PANC-1, SNU-213, and AsPC-1). (E) Cell viability assay for evaluating the effect of rNDV and rNDV-PTEN on the viability of normal and PDAC cell lines. The cells were infected with rNDV or rNDV-PTEN at a multiplicity of infection (MOI) of 1.0. For negative control, the cells were grown in the culture medium. After incubating for 96 h, cell viability assay was performed using a Cell Proliferation Assay kit. Data are presented as means ± standard deviation for independent experiments. $^{*}p < 0.05$, $^{**}p < 0.01$, $^{***}p < 0.001$ vs. control.

22,465 genes (first, Catenin Delta 2 [CTNND2]; second, glycine amidinotransferase [GATM] genes are not related to pancreatic cancer) in tissues of patients with pancreatic cancer, thereby confirming that AKT expression was increased. Based on this, we sought to treat pancreatic cancer by restoring decreased PTEN expression using rNDV-PTEN treatment.

Expression of PTEN, P-AKT, and P-mTOR in various PDAC cells and normal pancreatic cells

We conducted experiments to confirm the mRNA and protein expression of PTEN in normal pancreatic cells (hTERT-HPNE) and human pancreatic cancer cell lines (PANC-1, SNU213, AsPC-1). This was done to compare the results with those obtained from Figure S1, which shows the mRNA array data. PTEN mRNA levels in normal pancreatic (hTERT-HPNE) and PDAC (PANC-1, SNU-213, and AsPC-1) cell lines were determined using RT-qPCR (Figure 1A). The levels were significantly downregulated in PANC-1 cells. PTEN (Figure 1B), P-AKT (Figure 1C), and P-mTOR (Figure 1D) protein levels were evaluated in these cell lines using western blot analysis. PTEN protein levels were lower in PANC-1 cells than in other PDAC cell lines (SNU-213 and AsPC-1) or normal human pancreatic cells (hTERT-HPNE). The P-AKT and P-mTOR levels were highest in PANC-1 cells (Figures 1C and 1D). These results suggest that low PTEN protein expression influences the activation of the Akt/mTOR signaling pathway.

PDAC cell-killing effect of rNDV and rNDV-PTEN

We investigated the mechanism of cell death by treating hTERT-HPNE, PANC-1, SNU213, and AsPC-1 cell lines with oncolytic virus NDV, rNDV, and rNDV-PTEN, which contains PTEN cDNA, at a multiplicity of infection (MOI) of 1. The cancer cell-killing effect of rNDV-PTEN was 2.56-fold higher than that of rNDV in PANC-1 cells (Figure 1E). In SNU-213 and AsPC-1 cells, the killing effect of rNDV-PTEN was 2.04- and 1.61-fold higher than that of rNDV, respectively. These results suggest that PTEN induces a strong cancer cell-killing effect in PDAC cells.

Growth kinetics and PANC-1 cell-killing effect of rNDV and rNDV-PTEN

To investigate viral growth in PANC-1 cells, rNDV-PTEN and rNDV were used to infect PANC-1 (Figure 2A) and DF-1 (Figure S2) cells. The virus titers gradually increased in a time-dependent manner (Figure 2A). In PANC-1 cells, the viral titers of rNDV-PTEN and rNDV peaked at 96 h post infection (hpi) to $10^{5.25}$ and 10^{6} tissue culture infective dose 50 ($TCID_{50}$/mL), respectively. In DF-1 cells, growth of rNDV-PTEN and rNDV increased in a time-dependent manner and reached its highest titer at 96 hpi to $10^{6.25}$ and $10^{6.50}$ $TCID_{50}$/mL, respectively. rNDV replicates more rapidly than rNDV-PTEN, but the difference was not significant. Research has shown that, when PTEN expression is low, the initial immune response (interferon [IFN]-β, IFN-α) to viral infection in cells is reduced. These results suggest that PTEN insertion did not significantly affect virus growth in normal cell line such as the DF-1 cells and PANC-1 cells. The results of

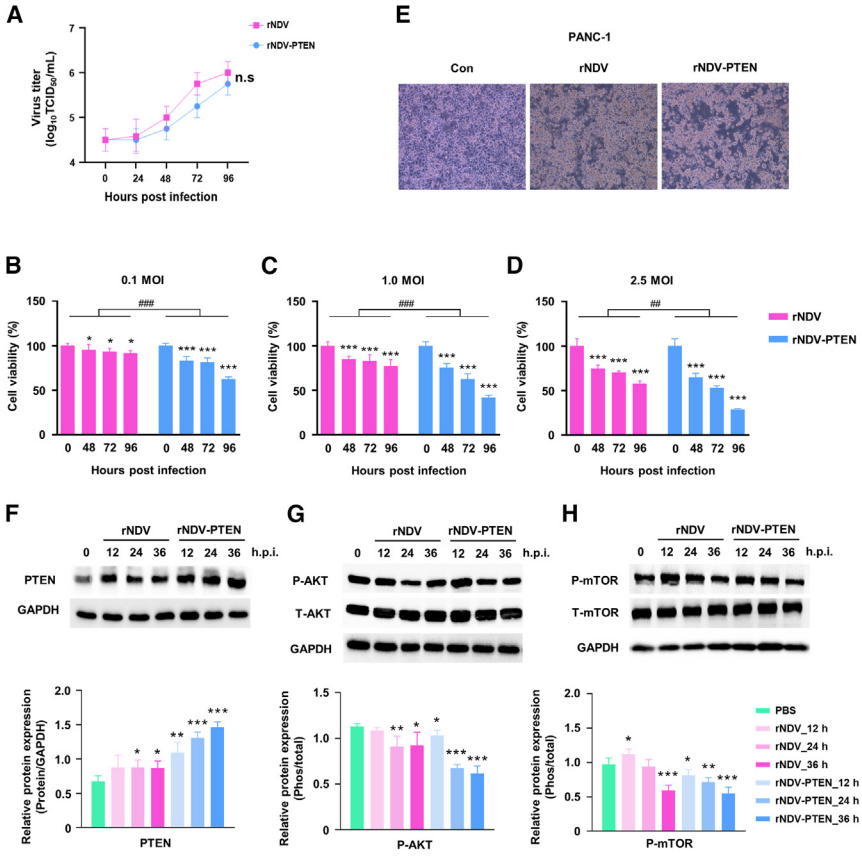

Figure 2. rNDV-PTEN effectively induces cell killing, upregulates PTEN, and downregulates P-AKT and P-mTOR

(A) Kinetics of rNDV and rNDV-PTEN multiplication in PANC-1 cells. The cells were infected with rNDV or rNDV-PTEN at 0.5 MOI. The supernatant was collected at 24, 48, 72, and 96 h post infection for $TCID_{50}$ titration. The graph depicts the mean $log_{10}TCID_{50}$/mL values. (B–D) MTT assay for evaluating the effect of rNDV and rNDV-PTEN on the viability of PANC-1 cells. PANC-1 cells were infected with rNDV or rNDV-PTEN at different MOIs (0.1, 1.0, and 2.5). After incubating for 48, 72, or 96 h, cell viability assays were performed using a Cell Proliferation Assay kit. (E) Micrographs showing the cytopathic effect of rNDV and rNDV-PTEN on PANC-1 cells at 36 h post infection. (F–H) Effect of rNDV or rNDV-PTEN infection on the levels of PTEN, P-AKT, and P-mTOR proteins. PANC-1 cells were infected with rNDV or rNDV-PTEN and harvested at 12, 24, and 36 h post infection. The protein levels were analyzed via western blot analysis using the respective antibodies. Data (A–D and F–H) are presented as means ± standard deviation for independent experiments. $^{*}p < 0.05$, $^{**}p < 0.01$, $^{***}p < 0.001$ vs. control; $^{\#}p < 0.05$, $^{\#\#}p < 0.01$, $^{\#\#\#}p < 0.001$ rNDV vs. rNDV-PTEN.

tetrazolium-based colormetric (MTT) assay showed that the cancer cell-killing effect was directly proportional to the MOI (Figures 2B–2D and S3A–S3C). The cancer cell-killing effect of rNDV-PTEN was higher than that of rNDV at 48, 72, and 96 hpi at an MOI of 0.1. At 96 hpi, the cancer cell viability for rNDV and rNDV-PTEN at 2.5 MOI was 57.86% and 28.80%, respectively, in PANC-1 cells ($p < 0.05$). The cell viability decreased in a time-dependent manner in PANC-1 cells infected with rNDV or rNDV-PTEN at an MOI of 2.5. The cancer cell-killing effect of rNDV-PTEN in PANC-1 cells was significantly increased by 1.68-fold compared with that of rNDV infection. The cytopathic effect (CPE) of rNDV- and rNDV-PTEN-infected PANC-1 cells was observed under a microscope at 36 hpi (Figure 2E). PANC-1 cells infected with rNDV-PTEN showed the most irregular cellular morphology compared with those infected with rNDV. These results indicate that rNDV-PTEN exhibits a significantly enhanced cancer cell-killing effect against PANC-1 compared to rNDV.

Effect of rNDV-PTEN infection on the expression of PTEN, P-AKT, and P-mTOR in PANC-1 cells

PTEN was overexpressed in rNDV-PTEN-infected PANC-1 cells (Figure 2F). The effect of PTEN overexpression on P-AKT and P-mTOR levels was assessed using western blotting (Figures 2G and 2H). The increase in PTEN through rNDV-PTEN treatment was found to reduce AKT phosphorylation compared to the rNDV-treated group as hpi time increased. However, there was no significant difference in mTOR phosphorylation between the rNDV-PTEN and rNDV treatment groups.

Effect of rNDV-PTEN infection on apoptotic and autophagic signaling pathways in PANC-1 cells

We investigated the effect of rNDV-PTEN on PANC-1 cell apoptotic signaling. Cleaved caspase 8 is extrinsic pathway of apoptosis signaling pathway, which upregulated in rNDV- and rNDV-PTEN-infected PANC-1 cells (Figure 3A). PTEN overexpression downregulated AKT and mTOR phosphorylation, which reduced BCL2 and increased Bcl-2-associated X protein (BAX) expression, resulting in an increased BAX/BCL2 ratio (Figure 3B). Increased levels of BAX protein are inserted into the mitochondrial membrane, which releases cytochrome *c* (Figure 3C). APAF1, in combination with cytochrome *c*, forms apoptosomes and initiates the binding of cleaved procaspase 9 (Figure 3D). Caspase 9-binding apoptosomes activate caspase 3 (Figure 3A). The levels of cleaved caspase 9 in PANC-1 cells infected with rNDV-PTEN were higher than those in cells infected with rNDV. These results indicated that rNDV-PTEN treatment induced both the intrinsic and extrinsic pathway of apoptosis; however, the extrinsic pathway showed no difference between rNDV-PTEN and rNDV treatment in PANC-1 cells.

rNDV and rNDV-PTEN infections induced AMP-activated kinase (AMPK) production (Figure 3E), and AMPK phosphorylated beclin

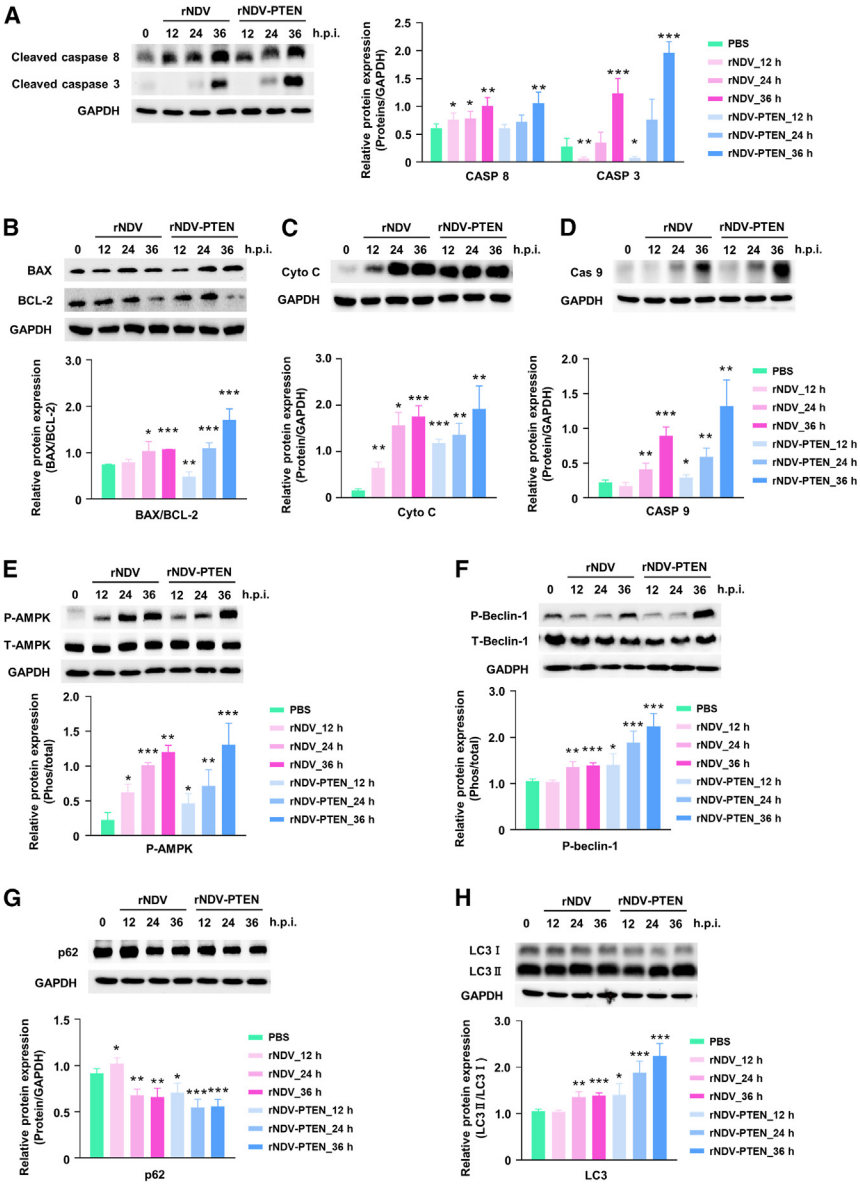

Figure 3. rNDV-PTEN induces tumor cell death via activation of apoptosis and autophagy in PANC-1 cells

(A–D) PANC-1 cells were infected with rNDV or rNDV-PTEN and harvested at 12, 24, and 36 h post infection. The rNDV- or rNDV-PTEN-induced apoptosis was analyzed via western blot analysis using antibodies against caspase 8, caspase 3, caspase 9, BAX, BCL2, and cytochrome *c*. (E–H) Effect of rNDV and rNDV-PTEN infection on autophagy-related proteins. The levels of autophagy-related proteins were analyzed via western blot analysis using antibodies against P-AMPK, T-AMPK, P-Beclin 1, T-Beclin 1, p62, and LC3 II. GAPDH expression was used as a loading control. The intensities of bands were analyzed by densitometry using ImageJ software, normalized against GAPDH expression, and presented as means ± standard deviation for independent experiments. $^{*}p < 0.05$, $^{**}p < 0.01$, $^{***}p < 0.001$ vs. control; $^{\#}p < 0.05$, $^{\#\#}p < 0.01$, $^{\#\#\#}p < 0.001$ rNDV vs. rNDV-PTEN.

1 (Figure 3F). The fusion (F) and hemagglutinin-neuraminidase (HN) proteins of NDV trigger autophagy via the activation of the AMPK-ULK1 pathway.[28] Studies indicate that NDV F and HN proteins can increase AMPK activation. rNDV and rNDV-PTEN treatments show elevated P-AMPK levels without significant differences between them, unlike beclin-1 phosphorylation. Based on the AMPK and phosphorylated beclin 1 expression, we examined the changes in p62 and LC3 II that participate in autophagosome formation. After NDV infection, p62 levels decreased (Figure 3G) but LC3 II levels increased (Figure 3H). The autophagy signaling pathway increased in the rNDV-PTEN-treated group compared to the phosphate-buffered saline (PBS) group; however, there was no significant difference when compared to the rNDV-treated group. Taken together, these results suggest that the restoration of PTEN via rNDV-PTEN treatment, in addition to the effects of rNDV such as extrinsic pathway of apoptosis and autophagy activation, induces the intrinsic pathway of apoptosis.

rNDV-PTEN suppresses tumor growth in LTPA syngeneic mouse model

To investigate the antitumor effects of rNDV-PTEN, a syngeneic mouse model was established using LTPA cells derived from mouse pancreatic cancer (Figure 4A). We aimed to demonstrate the suppression of pancreatic tumor growth via PTEN expression following rNDV-PTEN treatment. The average tumor volume in all groups was approximately 120 mm^3 27 days after injecting cancer cells. Figure 4B shows the changes in tumor volume from 27 to 37 days during virotherapy. Tumor volume decreased in both the rNDV- and rNDV-PTEN-inoculated groups, with the rNDV-PTEN-inoculated group showing the highest reduction. Tumor changes during virotherapy were monitored from 27 to 37 days and tumor tissue volume was observed at 3 and 7 days post virotherapy (Figures S4A and S4B). Tumor volume at day 7 post virotherapy was 78.95 mm^3 in the rNDV-PTEN group, 95.55 mm^3 in the rNDV group, and 133.65 mm^3 in the PBS group.

PTEN expression was clearly observed in the tumor tissue in the rNDV-PTEN-inoculated group, and HN protein was detected in the tumor tissue of the rNDV- or rNDV-PTEN-inoculated group (Figure 4C). Tumor-selective replication of rNDV and rNDV-PTEN was validated using qPCR analysis based on the mRNA levels of the M protein and PTEN. Significantly higher levels of NDV

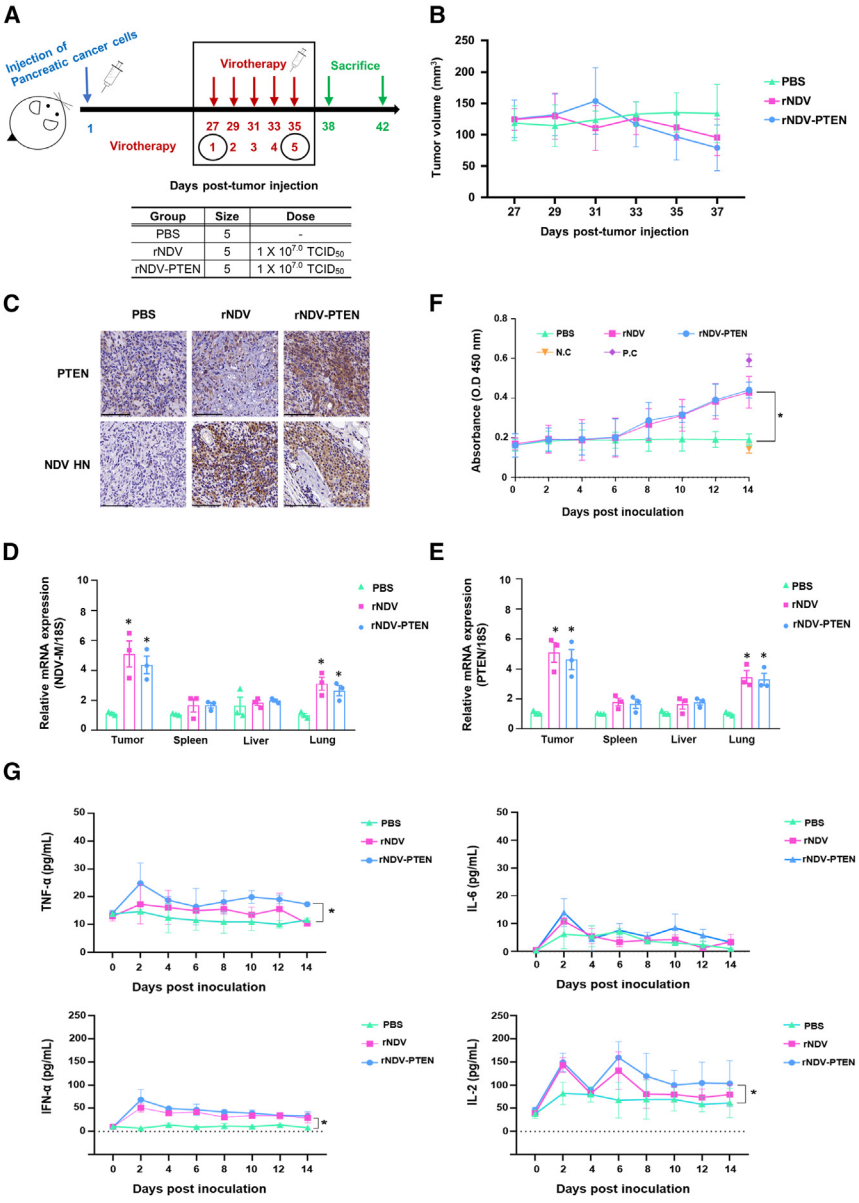

Group	Size	Dose
PBS	5	-
rNDV	5	1 X $10^{7.0}$ $TCID_{50}$
rNDV-PTEN	5	1 X $10^{7.0}$ $TCID_{50}$

Figure 4. rNDV-PTEN inhibits tumor cell proliferation and metastasis in LTPA syngeneic model

(A) Syngeneic model construction and virus administration. Mice were subcutaneously injected with LTPA cells. After 27 days of tumor cell injection, the mice were i.v. inoculated with PBS, rNDV, or rNDV-PTEN, every 2 days, a total of five times. (B) Tumor size was monitored via caliper measurements every 2 days (C) Immunohistochemical staining of PTEN and HN in tumor tissue in LTPA syngeneic mice. Scale bar: 100 μm. (D and E) The mRNA expression of PTEN and NDV-M (M gene of NDV) in the tumor, spleen, liver, and lung was measured by using qPCR. 18s was used as an internal control. (F) OD value on measurement of NDV ELISA antibody in LTPA syngeneic mice. (G) Measurement of serum cytokine levels (TNFA, IFNA, IL2, and IL6) in LTPA syngeneic mice. Data are presented as means ± standard deviation. *$p < 0.05$, **$p < 0.01$, ***$p < 0.001$ vs. PBS-injected mice.

(Figure 4D) and PTEN (Figure 4E) mRNAs were detected in the tumor, spleen, liver, and lungs. In particular, the mRNA levels of rNDV-PTEN were higher than those of rNDV. These results corroborated the fact that rNDV-PTEN replicated more than rNDV did in PANC-1 cells (Figure 2A).

Analysis of immune response to rNDV-PTEN in the LTPA syngeneic mouse model during virotherapy

To investigate NDV HN enzyme-linked immunosorbent assay (ELISA) antibody formation and changes in inflammatory cytokines following intravenous administration of rNDV-PTEN in the LTPA syngeneic mouse model. ELISA was performed to evaluate HN protein-specific antibody titers and cytokine levels generated by virotherapy. The NDV HN antibody test using blood collected from day 0 to day 14 post virus injection was conducted to verify the formation of antibodies against the virus, which was administered five times every 2 days. Particularly, the biodistribution results of the virus in mice sacrificed at 14 days post inoculation (fifth 7 dpv-days post virotherapy) showed that NDV-M mRNA and PTEN were detected in tissues (Figures 4D, 4E, 6B, and 6C). Fourteen days is considered sufficient time for antibody formation due to the normal immune response of C57BL/6 mice, as opposed to immunocompromised nude mice. When the serum dilution was adjusted to 1:50, ELISA detected antibodies at levels comparable to those observed in mouse vaccination experiments using NDV, which were within the acceptable range (Figure 4F). TNF-alpha (TNFA), interferon-alpha (IFNA), interleukin (IL)2, and IL6, the primary cytokines for the immune response against viral infections, were monitored during the virotherapy (Figure 4G). The TNFA concentration increased in the rNDV (17.30 pg/mL) and rNDV-PTEN (24.84 pg/mL) groups compared with that in the PBS group (14.69 pg/mL) 1 day after the first virotherapy. The level of TNFA in the rNDV-PTEN group was slightly higher than that in the rNDV or PBS group from the second virotherapy to the fifth virotherapy. The level of IFNA was upregulated in the rNDV (51.33 pg/mL) and rNDV-PTEN (63.45 pg/mL) groups 1 day after the first virotherapy. However, the level of IFNA was restored from the second to fifth virotherapy. IL2 plays an important role in the activation of T cells during virus infection.[29] IL2 expression increased in the rNDV (143.11 pg/mL) and rNDV-PTEN (149.04 pg/mL) groups compared with that in the PBS group (82.07 pg/mL) 1 day after the first virotherapy.

IL2 levels decreased following virotherapy; nonetheless, the levels in the rNDV and rNDV-PTEN groups were slightly higher than those in the PBS group. IL6 levels increased slightly in the rNDV and rNDV-PTEN groups compared with those in the PBS group. IL6 concentrations, measured on the day after the first virotherapy, were 17.31, 4.23, and 6.28 pg/mL in the rNDV-PTEN, rNDV, and PBS groups. The average IL6 concentrations were 4.90, 2.77, and 5.31 pg/mL in the PBS, rNDV, and rNDV-PTEN groups, respectively.

rNDV-PTEN suppresses tumor growth in a xenograft mouse model of PANC-1 cells

To demonstrate the tumor-suppressive effect of rNDV-PTEN, an *in vivo* assay was performed using a PANC-1 xenograft mouse model. rNDV, rNDV-PTEN, and PBS were intravenously (i.v.) injected into tumor-bearing mice, every 2 days, for a total of 10 injections from day 15 to day 33 (Figure S5A). Figure S5B shows the changes in tumor volume from 1 to 35 days after injecting tumor cells. Tumor growth was suppressed upon injection of rNDV and rNDV-PTEN. After completion of virotherapy, the tumor tissue from the rNDV-PTEN-injected mice showed the smallest volume (Figure S5C). The tumor volumes of 131.44 and 62.68 mm^3 in the rNDV and rNDV-PTEN groups were significantly smaller than those in the PBS-injected group (376.78 mm^3). Hematoxylin-eosin (H&E) staining revealed greater necrosis in the rNDV-PTEN group than in the rNDV group (Figure S5D). We investigated the mRNA expression of NDV matrix genes (NDV-M) and PTEN using qPCR. The mRNA expression of NDV-M and PTEN was significantly induced in the tumor tissue but did not increase in the spleen, liver, or lung tissues compared with that in the tumor (Figures S5E and S5F). These results indicate that PTEN-harboring rNDV has a stronger tumor-suppressive effect on PDAC than rNDV.

rNDV-PTEN suppresses tumor growth in an orthotopic mouse model of PANC-1 cells

To determine whether PTEN overexpression significantly inhibits the proliferation of PANC-1 cells in an *in vivo* orthotopic mouse model, we orthotopically xenografted PANC-1-Luc2 cells into BALB/c nude mice (Figure 5A). At 22 days after cell injection, we initiated virotherapy using rNDV, rNDV-PTEN, and PBS administered via intravenous injection. No significant differences were observed in the body weights of the three groups (Figure 5B). The timing of tissue harvest was based on the humane tumor endpoint criteria, consisting of both tumor size (both width and length more than 2 cm). Tumor-free weight increased in the rNDV-PTEN group compared with that in the PBS group (Figures 5C and 5D). These results indicated that a certain proportion of the body weight of mice in the PBS group was due to the tumor cells. To measure the *in vivo* efficacy of PTEN overexpression on tumor growth in the PANC-1 mouse model, we detected in vivo imaging system (IVIS)-luciferase activity in tumor scans, 3 (before virotherapy) and 8 (18^{th} virotherapy) weeks after tumor injection. The results of IVIS-luciferase activity showed significantly decreased tumor growth in rNDV-PTEN-treated mice compared with that in rNDV and PBS mice (Figure 5E). We investigated whether rNDV effectively delivered PTEN mRNA to the tumor tissue as well as the expression of HN and PTEN in pancreatic tumor tissues using immunohistochemistry. As expected, the expression of HN and PTEN was increased in the tumor tissues of rNDV-PTEN-treated mice compared with that in PBS-treated mice (Figure 5F). H&E staining of paraffin-embedded tumor sections from PBS-treated, rNDV-treated, and rNDV-PTEN-treated mice revealed compact and loose epithelial cells in rNDV-PTEN-treated mice (Figure 5F). Staining of tumor sections using antibodies against Ki67, a marker of tumor cell proliferation in various cancers, revealed lower proliferation (lesser brown stain) in the rNDV-PTEN group than in the PBS-treated group (Figure 5F). Tumor sections from rNDV-PTEN-treated mice exhibited less neovascularization (CD31, brown) and lower metastatic index (MMP9, brown) than in PBS-treated mice (Figure 5F). To confirm that the virus had reached the pancreatic cancer tissue, the sections were costained with pancreatic cancer markers CA19-9 and HN, and the images were merged. The patterns of reactivity with these virus markers in pancreatic cancer were similar to those observed in rNDV-PTEN- and rNDV-treated mice (Figure 6A). To investigate the side effects of rNDV-PTEN and rNDV treatment in mice, we performed blood analysis of PBS- and rNDV-PTEN-treated mice. The kidney and liver functions were evaluated based on the measurement of creatinine (CREA), and aspartate aminotransferase (AST) and alanine aminotransferase (ALT) levels, respectively. No significant differences were observed among the three groups, and the values were within the normal range (Figure S6). However, glucose (GLU) metabolism disrupted by pancreatic cancer was restored by rNDV-PTEN administration, and blood GLU and triglyceride (TRIG) levels were significantly reduced. We also examined the mRNA expression of NDV matrix gene (NDV-M) and PTEN using qPCR. Although the mRNA expression of NDV-M and PTEN was significantly induced in tumor tissues, there was no significant change in other tissues (spleen, liver, and lung) (Figures 6B and 6C). The expression of PTEN at the protein level was the same as its mRNA expression (Figure 6D). These results indicated that rNDV-PTEN effectively reached the tumor tissue, induced PTEN expression, and suppressed tumor cell proliferation and metastasis.

rNDV-PTEN treatment attenuated PI3K/AKT/mTOR signaling pathway via PTEN overexpression

Generally, AKT and mTOR activation are related to cellular homeostasis, proliferation, and survival in several cells.[30] We verified the mechanism by which rNDV-PTEN induces apoptosis via regulation of the PI3K/AKT/mTOR signaling pathway in the orthotopic mouse model of PANC-1. As expected, rNDV-PTEN treatment decreased the phosphorylation of AKT (S473) and mTOR (S2448) but increased the phosphorylation of AMPK (Th172) (Figure 7A). Inhibition of the PI3K/AKT/mTOR pathway induced autophagy through beclin 1 phosphorylation, decreased p62 expression, and increased LC3 I/II ratio (Figure 7B). In the tumor tissue from rNDV-PTEN-treated mice, BCL2 expression was decreased by beclin 1 phosphorylation. We also assessed the changes in the levels of apoptotic protein markers and found a

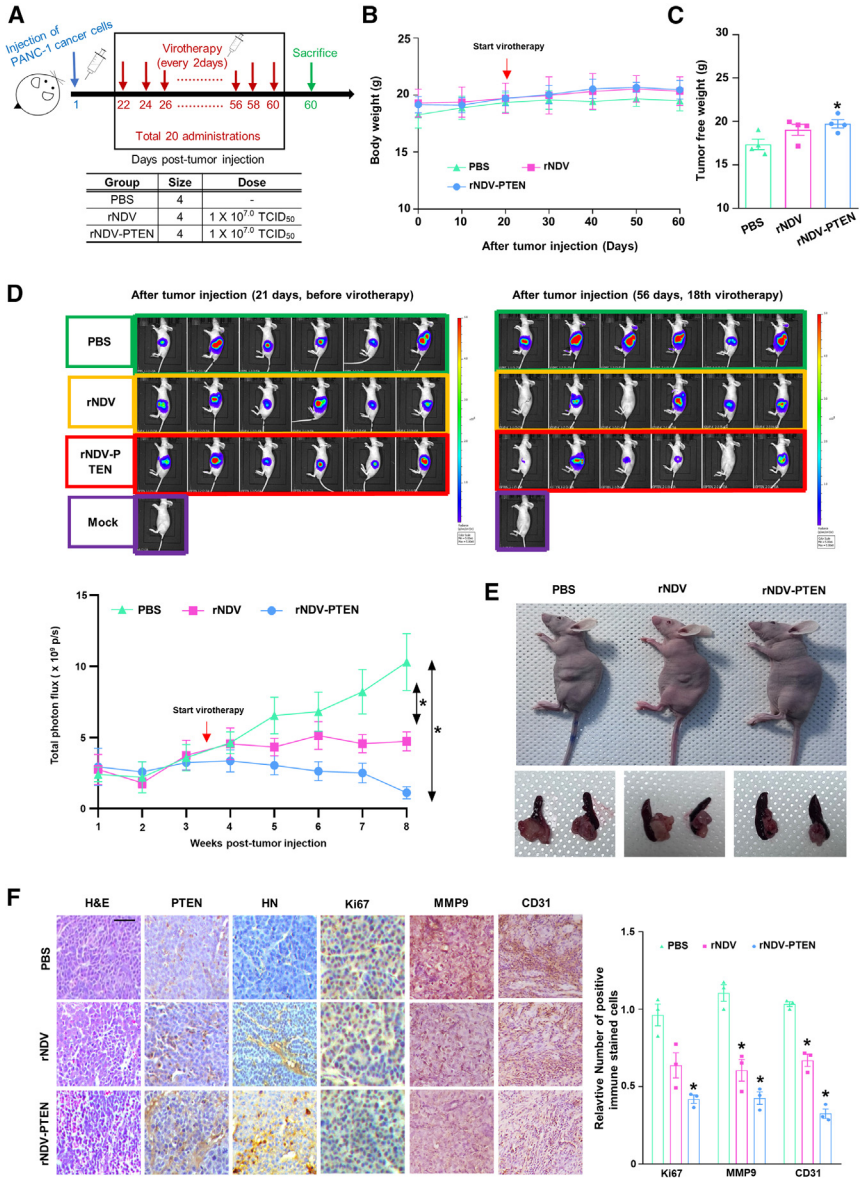

Figure 5. rNDV-PTEN inhibits tumor cell proliferation and metastasis in PANC-1 orthotopic model

(A) Five-week-old female BALB/c nu−/nu− mice were anesthetized using 250 mg/kg 2,2,2-tribromoethanol (Avertin), and then 5 × 10^4 PANC-1-Luc2 cells were injected as follows: an approximately 3-cm incision was made on the left side of the abdomen, the spleen was lifted to expose the pancreas, and 100 μL of the cell suspension was injected using an insulin syringe. After 22 days of tumor cell injection, the mice were i.v. inoculated with PBS or rNDV, or rNDV-PTEN, every 2 days, a total of 20 times. (B) Body weight of orthotopic model mice. (C) Tumor-free weight of orthotopic model mice after sacrifice at 60 days post tumor injection. (D) Bioluminescent images of luciferase activity of PANC-1 cells. Bioluminescent images were taken with IVIS lumina XR and analyzed using Living Image software (n = 6). (E) Photographs of mice bearing tumors and tumor after isolation from the mice. (F) Hematoxylin-eosin (H&E) and immunohistochemical staining of PTEN, HN, Ki67 (proliferation marker), MMP9 (metastasis marker), and CD31 (angiogenesis marker) in tumor tissue in the pancreas of orthotopic model mice. Scale bar: 50 μm. Data are presented as means ± standard deviation for independent experiments. *p < 0.05 vs. PBS-injected mice.

significant induction of cleaved caspase 3 and 8, BAX, and cleaved caspase 9 (Figure 7C). The autophagy signaling pathway and PI3K/AKT/mTOR signaling pathway increased in the rNDV-PTEN-treated group compared to the PBS group; however, there was no significant difference when compared to the rNDV-treated group. Taken together, these results were consistent with the findings from *in vitro* experiment (Figures 2 and 3), which means that the restoration of PTEN via rNDV-PTEN treatment triggers the intrinsic pathway of apoptosis.

DISCUSSION

The development of cancer therapeutics that employ a gene-based approach has spurred the realization that specific genes are closely involved in the occurrence and progression of cancer.[31] Several genes are simultaneously involved in the occurrence and progression of cancer.[32]

PTEN is a multifunctional protein that regulates cell growth, survival, and various signaling pathways. Its primary functions are often associated with tumor suppression and control of cell proliferation. PTEN has also been implicated in the regulation of GLU metabolism and maintenance of metabolic homeostasis, although it is involved in mitochondrial function. PTEN mutations are rare in pancreatic cancer; however, low PTEN expression levels affect pancreatic cancer development. In this study, we used three types of PDAC cells with KRAS mutations and low PTEN expression. PTEN gene sequencing results did not show any mutation in PTEN (Figure S7). PTEN expression was measured at the mRNA and protein levels (Figures 1A and 1B). The mRNA levels were not significantly different between normal cells and PDAC, with the exception of Panc-1 cells, in which the expression was slightly lower than that in normal cells. Nonetheless, Panc-1 cells had very low levels of PTEN protein relative to that in normal cells, and the PTEN protein levels in SNU-213 cells were half those in normal cells without a difference at the mRNA level (Figure 1B). There are several possible reasons why protein expression is reduced even in the absence of a mutation in PTEN. All pancreatic cancer cell lines used in our study have mutations in the p53 gene, as well as in KRAS.[33] Studies have shown that p53 mutations are related to reduced PTEN expression, although their relationship with KRAS

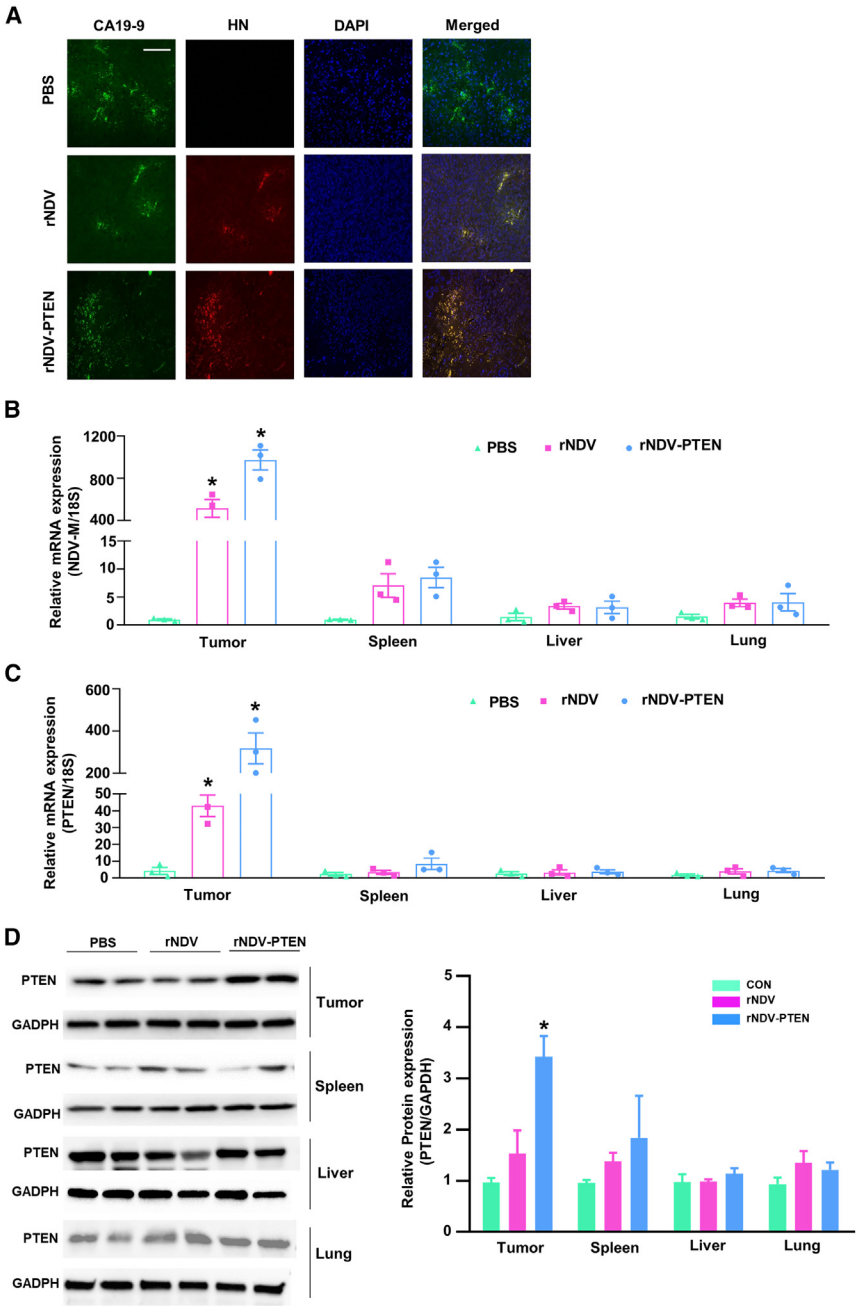

Figure 6. rNDV-PTEN effectively infects the tumor cells and overexpresses PTEN without affecting other tissues in PANC-1 orthotopic model

(A) Immunofluorescence staining of CA19-9 (pancreatic cancer marker) and HN in tumor tissue in the pancreas of orthotopic model mice. Scale bar: 50 μm. (B and C) mRNA expression of PTEN and NDV-M (NDV matrix gene) measured using qPCR. The expression of 18S was used as an internal control. (D) PTEN expression in several tissues measured using immunoblotting. GAPDH expression was used as an internal control. The protein levels were quantified densitometrically using ImageJ software (right panel). Data are presented as means ± standard deviation for independent experiments. *$p < 0.05$ vs. PBS-injected mice.

(Figures 2B–2D, 4B, and 5D). The PTEN gene was transported by rNDV into PANC-1 cells, resulting in cytoplasmic accumulation of the protein, which blocked the PI3K/AKT/mTOR signaling pathway and triggered the apoptotic pathway. An increase in the levels of apoptotic proteins was observed *in vitro* and *in vivo* (Figures 3A–3D). It has been clearly revealed that PTEN enhances the killing effect of pancreatic cancer cells through an apoptosis activation mechanism. PTEN overexpression altered the levels of autophagy-related signaling pathway proteins to activate autophagy (Figures 3E–3H). mTOR is a key component of this pathway whose activation inhibits autophagy. In contrast, autophagy is initiated when mTOR is inhibited. AKT is a serine/threonine kinase that acts downstream of PI3K. Activated AKT inhibits the tuberous sclerosis complex 2 (TSC2), which normally inhibits mTOR. TSC2 inhibition leads to the activation of mTOR, which suppresses autophagy.[36] PI3K is an upstream activator of AKT. Inhibition of PI3K can lead to decreased activation of AKT and subsequent downregulation of mTOR, promoting autophagy.[37]

mutations has not been elucidated.[34] Low PTEN expression is linked to the development of various cancers,[35] including pancreatic cancer. In addition to p53 mutations, identification of other factors related to reduction in PTEN levels and its relation to development, progression, and severity of pancreatic and other cancers requires intensive research.

In the present study, we demonstrated that restoration of PTEN in pancreatic cells enhances cancer cell death and tumor suppression

PTEN inhibits AKT phosphorylation, leading to AMPK activation, which in turn inhibits mTOR and activates ULK1 and beclin 1, promoting autophagy through a series of phosphorylation events.[38] We propose that NDV infection induces endoplasmic reticulum (ER) stress, forming the ULK1/2 complex and inhibiting mTOR, thereby activating autophagy. In NDV-infected cancer cells, ER stress disrupts the beclin 1-BCL2 complex, releasing beclin 1 to further activate autophagy. Beclin1 phosphorylation prevents BCL2 expression, inducing apoptosis, as BCL2 is an anti-apoptotic protein.[39] While autophagy typically activates when this pathway is inhibited, it can have both

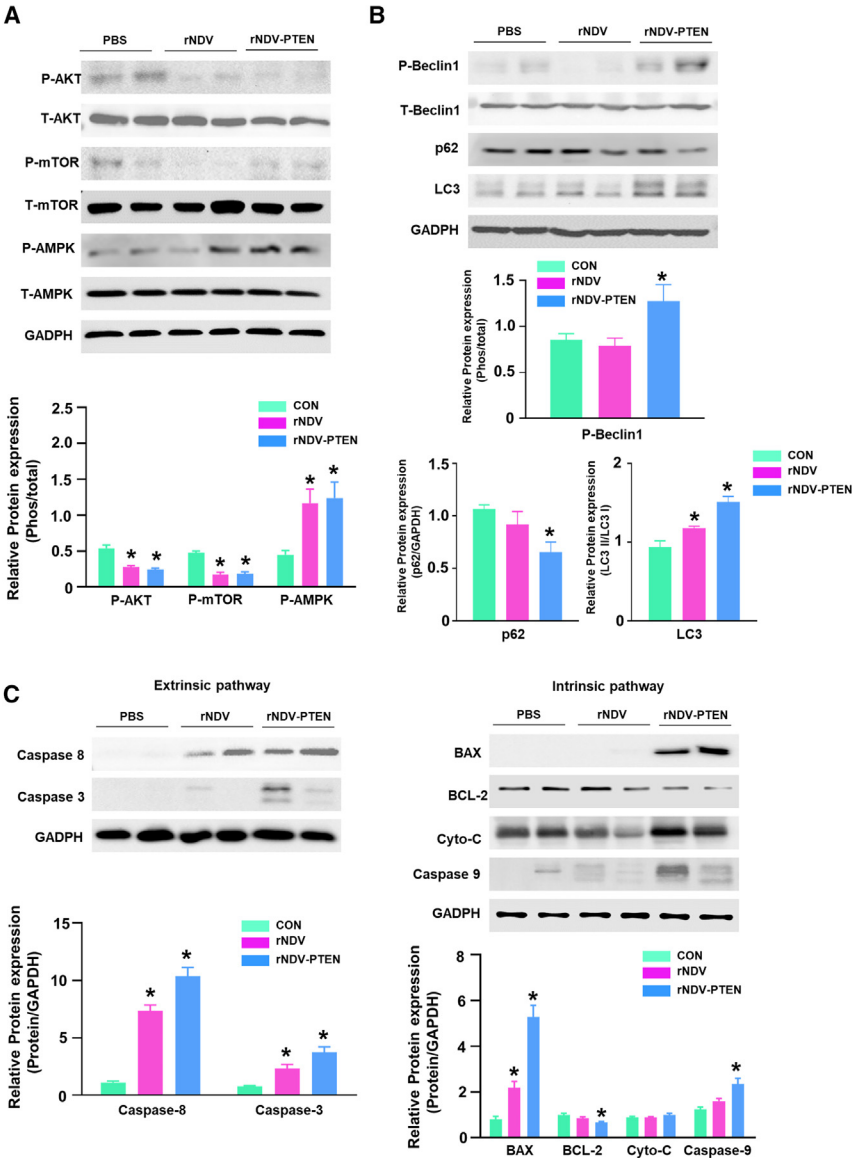

Figure 7. rNDV-PTEN induces tumor cell death via activation of apoptosis and autophagy in PANC-1 orthotopic model

(A) Expression of proteins in the PI3K/AKT/mTOR and AMPK signaling, (B) autophagy, and (C) apoptosis pathways was measured using immunoblotting in tumor tissues in the pancreas of orthotopic model mice. GAPDH expression was used as an internal control. The protein levels were quantified densitometrically using ImageJ software (bottom panel). Data are presented as means ± standard deviation for independent experiments. *$p < 0.05$ vs. PBS-injected mice.

tumor-suppressive and tumor-promoting roles, depending on the cancer type and its stage.

Our study showed that rNDV containing the PTEN gene enhanced tumor inhibition in PDAC by activating autophagy-related signaling proteins. NDV infection induces autophagy and increases apoptosis in cancer cells. However, its specific effects on pancreatic cancer remain underexplored. Although PTEN restoration plays a significant role in triggering apoptotic pathways, it is also likely that the cytotoxic response observed is influenced by factors beyond PTEN expression alone. The infection efficiency and replication potential of rNDV may vary across different PDAC cells, contributing to differences in the overall tumor lysis effect. This suggests that rNDV's ability to target and kill cancer cells may depend not only on PTEN but also on the virus's interaction with cellular factors that affect its efficacy. We observed changes in signaling proteins related to autophagy, including P-Beclin1, LC3, and p62; however, further research is needed to understand these interactions and their implications for pancreatic cancer development.

Monitoring the immune response to rNDV carrying the PTEN gene in C57BL/6 mice revealed a weak humoral and cellular immune response. An NDV HN antibody test using blood collected from days 0–14 post virus injection was conducted to verify the formation of antibodies against the virus, which was administered five times at 2-day intervals. In particular, the biodistribution results of the virus in mice sacrificed 14 days post inoculation (after fifth 7 dpv) showed that NDV-M mRNA was more frequently detected in tissues than in major organs (Figures 4D, 4E, 6B, and 6C). A 14-day period is generally sufficient for antibody formation in C57BL/6 mice, given their normal immune response, unlike in immunocompromised nude mice. Serum was diluted 1:50 according to the kit's sample preparation method. At this dilution, the ELISA detected antibodies at levels comparable to those observed in mouse vaccination experiments using NDV, which were within the acceptable range. The virus can be translated into rNDV and replicated in tumor cells, but not in normal cells. In addition, the levels of ALT, AST, CREA, and cholesterol in the blood were not significantly different, while GLU and TRIG levels were decreased in the rNDV-PTEN-injected group (Figure S4). We established a pancreatic cancer xenograft model and an orthotopic mouse model using luciferase-tagged PANC-1-Luc2 cells. In the orthotopic mouse model, we administered rNDV-PTEN via intravenous injection and confirmed the presence of the HN protein and the transferred PTEN gene in tumor tissues using qPCR and western blotting. Additionally, changes in the luciferase activity of pancreatic cancer cells were monitored using IVIS, which revealed significantly improved antitumor effects in the rNDV-PTEN group compared

with the rNDV and PBS groups. This indicates the potential of the intravenous administration of rNDV-PTEN to achieve antitumor effects in pancreatic cancer, particularly where direct injection is not feasible. Our *in vivo* results suggest that, while PTEN restoration likely plays a key role in the observed antitumor effects, other factors, such as the efficiency of viral infection and replication within tumor cells, may also contribute to tumor shrinkage. These viral kinetics, including the infection efficiency and replication rate, likely enhance the therapeutic effect of rNDV-PTEN. Therefore, the combination of PTEN expression and enhanced viral proliferation likely maximizes the overall antitumor response.

Although we demonstrated that the rNDV-PTEN virus exhibited an increased tumor-suppressive effect in the PDAC animal model, we also identified significant challenges that need to be addressed through further research. To explore effective pancreatic cancer treatment strategies, we tested n intravenous injection route in this study. Intravenous administration may lead to challenges such as loss owing to incomplete virus delivery to cancer cells and rapid viral clearance from the bloodstream. To maintain effective concentrations, we tested various injection frequencies: once every 2 weeks, weekly, once every 3 days, and once every 2 days. The most effective anticancer efficacy was observed when injections were administered every 2 days (data not shown). However, these results solely depend on injection frequency, not considering various virus concentrations per dose. Considering safety, virus concentration needs to be determined through appropriate testing for potency and toxicity evaluation to establish the optimal injection concentration, frequency, and interval. There are several references to clinical trials for brain tumor treatment using NDV.[40,41] These studies involved administering NDV to brain tumor patients either every other day for 20 days or twice a week, following protocols where the amount of NDV-HUJ was gradually increased. This was designed to ensure the sustained presence and activity of the virus necessary to maintain therapeutic levels and prevent virus clearance, in contrast to direct tumor injections. For instance, in the study "Phase I/II Trial of Intravenous NDV-HUJ Oncolytic Virus in Recurrent Glioblastoma Multiforme," patients were given NDV-HUJ i.v. with dosages that escalated over time. This protocol was implemented to ensure continuous viral presence and activity, which is crucial for effectively targeting and eliminating cancer cells. These protocols aim to maintain the virus in the bloodstream, providing a consistent therapeutic level that maximizes the oncolytic effects against tumors. These clinical trials provide essential insights into the potential of NDV as a therapeutic agent for various cancer types, including glioblastoma multiforme.

Another shortcoming of this study is that the absence of significant differences in apoptotic signaling proteins between rNDV-PTEN and rNDV, despite observing significant differences in the PDAC cell-killing effect and tumor-suppression effect in an animal model. In the case of P-Akt (Figure 2G), P-mTOR (Figure 2H), and cleaved caspase-8 (Figure 3A), extrinsic apoptosis pathway protein, there were no notable changes observed. We consider that this is due to the rNDV also having cancer cell-killing effect without the PTEN gene. NDV infection and replication in the cancer cells stimulate cancer cell lysis as well as some of the proteins of NDV directly engaging in several cancer cell-killing pathways.[25] NDV infection stimulates type I IFNs and it induces the p53-mediated intrinsic apoptosis pathway. NDV infection induced ER stress and it activated caspase 12 and caspase 3, resulting in apoptosis. NDV structural proteins, for example HN protein, were involved in stimulating apoptotic signaling in cancer cells.[42] Further studies on the mechanism of cancer cell death at the molecular level should be well designed and conducted. Nevertheless, the cancer cell-killing effect of lentogenic (non-pathogenic) NDV strains is known to be less than that of pathogenic strains, and, as a complement to this, there is enough value and usefulness to conduct research and development of oncolytic viruses using recombinant NDV harboring a tumor-suppressor gene.

In conclusion, rNDV-PTEN demonstrated a strong tumor-suppressive effect in PDAC, which was attributed to the abnormally activated PI3K/AKT/mTOR signaling pathway resulting from KRAS mutations and the loss of PTEN. Further studies using patient-derived PDAC cells with the same genetic background, along with more extensive animal safety tests, are required to fully assess the potential of rNDV-PTEN as a therapeutic for PDAC. Therefore, PTEN gene-containing rNDV may be a promising candidate for pancreatic cancer treatment.

MATERIALS AND METHODS

Experimental model and subject details

Cell lines and cell cultures

Human pancreatic (AsPC-1, PANC-1, and SNU-213) and African green monkey kidney (Vero) cells were purchased from the Korean Cell Line Bank (KCLB, Republic of Korea). Chicken embryonic fibroblast (DF-1), human larynx carcinoma (Hep-2), mouse pancreatic adenocarcinoma (LTPA), PANC-1-Luc2, and pancreatic ductal cell (hTERT-HPNE) cells were purchased from American Type Culture Collection (ATCC, USA). AsPC-1 and SNU-213 cells were cultured in RPMI1640 medium supplemented with 10% (v/v) fetal bovine serum (FBS, Sigma-Aldrich), 1% (v/v) penicillin-streptomycin solution (10,000 units/mL of penicillin and 10,000 μg/mL of streptomycin, PS, Gibco, Billings, MT, USA). hTERT-HPNE, PANC-1, and Vero cells were cultured in Dulbecco's modified eagle medium (DMEM) supplemented with 10% FBS and 1% PS. Hep-2 cells were cultured in MEM supplemented with 10% FBS and 1% PS.

Virus culture

Previously constructed rNDV and rNDV-PTEN were used in this study.[43] DF-1 cells (total 20 mL, $2.5 \times 10^{5.0}$ cells/mL) were seeded in T75 flasks at 37°C and cultured in an atmosphere of 5% CO_2. For rNDV or rNDV-PTEN infection, a monolayer of DF-1 cells was washed with PBS two times, and the virus was added at an MOI of 0.5 in serum-free DMEM with 1% PS (5 mL). The cells were washed with PBS to remove unbound virus at 1 hpi. The viruses were harvested 2 days post infection and stored at −80°C for subsequent analysis.

Animal ethics

The subcutaneous PANC-1 xenograft mouse model was approved by the Animal Care and Use Committee of Libentech (LBT-IACUC-AE-2021-04). Throughout the study, the mice were housed under controlled conditions, with an ambient temperature of 22°C ± 1°C and a light/dark cycle of 12 h. They were provided free access to sterilized food and water and monitored regularly for signs of distress or adverse effects. A body-weight reduction of 20% or more was considered a humane endpoint, at which the mice were sacrificed to minimize potential suffering and ensure animal welfare during the experimental period.

The subcutaneous LTPA syngeneic and PANC-1 orthotopic mouse models used in this study were approved by the Institutional Animal Care and Use Committee of Chungnam National University Hospital (CNUH-022-A0042) and adhered to the guidelines. Mice were maintained under a controlled environment (ambient temperature, 22°C–24°C; relative humidity, 50%–60%; 12-h light/dark cycle). A body-weight reduction of 20% or more was considered a humane endpoint, at which the mice were sacrificed in accordance with animal ethics.

Method details

Sample preparation for qPCR and western blotting

The normal (hTERT-HPNE, 1×10^5 cells/mL) and PDAC (PANC-1, SNU-213, and AsPC-1, 2×10^5 cells/mL) cells (total 2 mL) were seeded in a six-well plate (SPL, Republic of Korea) and cultured overnight at 37°C in an atmosphere of 5% CO_2. The cells were washed with PBS and centrifuged at 2,000 × *g* for 10 min at 4°C. Cell pellets were used for RT-qPCR and western blot analyses.

Preparation of virus-infected PANC-1 cell samples

PANC-1 cells (total 20 mL; $2.5 \times 10^{5.0}$ cells/mL) were seeded in a T75 flask (catalog #: 070075, SPL) and cultured overnight at 37°C in an atmosphere of 5% CO_2. The cells were infected with rNDV or rNDV-PTEN at an MOI of 2.5. The virus-infected cells were harvested at 12, 24, and 36 hpi and centrifuged at 2,000 × *g* for 10 min at 4°C. The cell pellet was resuspended in 500 μL of 10% radio immuno precipitation assay (RIPA) buffer (Sigma-Aldrich), and homogenized with an ultrasonic homogenizer (QSonica, USA). The cell homogenate was used for western blot analysis.

Western blot analysis

Protein samples (400 μL) were mixed with 100 μL of 5× sample buffer (250 mM Tris-HCl pH 6.8, 5% 2-mercaptoethanol, 10% sodium dodecylsulfate [SDS], 0.5% bromophenol blue, 50% glycerol). The mixture was denatured at 100°C for 3 min and then subjected to SDS-polyacrylamide gel electrophoresis (SDS-PAGE). Subsequently, the separated proteins were transferred onto a polyvinylidene difluoride membrane using a Power Blotter (catalog #: PB0012, Thermo Fisher Scientific, Waltham, MA, USA) at 25 A for 15 min. The membranes were blocked with 1% bovine serum albumin for 1 h (25°C ± 1°C) and probed with the appropriate antibody. The antibodies and their dilutions were as follows: anti-GAPDH (sc-32233; 1:1,000, Santa Cruz Biotechnology, Santa Cruz, USA); anti-LC3 (NB100-2220; 1:1,000, Novos Bio, USA); anti-P-mTOR Ser2448 (2971S; 1:1,000), anti-mTOR (2972S; 1:1,000), anti-P-AKT Ser473 (9271S; 1:1,000), anti-AKT (9272S; 1:1,000), anti-cleaved Cas3 (9664S; 1:1,000), anti-p62 (5114S; 1:1,000), anti-AMPK (2532S; 1:1,000), anti-P-AMPK Thr172 (2535S; 1:1,000), anti-Beclin 1 (3738S; 1:1,000), and anti-P-Beclin 1 Ser15 (84966S; 1:1,000) from Cell Signaling Technology (USA) and anti-Bcl-2 (ab182858; 1:500), anti-Bax (ab270742; 1:1,000), anti-cytochrome *c* (ab133504; 1:1,000), anti-caspase8 (ab220171; 1:500), anti-caspase-9 (ab202068; 1:1,000), and anti-PTEN (ab32199; 1:1,000) from Abcam (UK). After incubation with the primary antibody, the membranes were treated with appropriate horseradish peroxidase (HRP)-conjugated secondary antibodies and a 1:1 mixture of enhanced chemiluminescence substrate solutions A and B. The images were of blots were captured using the ChemiDoc MP Imaging System (catalog #: 17001402 Bio-Rad, Hercules, CA, USA), and the band densities were semiquantitatively analyzed using ImageJ V.1.8.0. Protein expression levels were normalized to those of GAPDH, which was used as a loading control.

Real-time qPCR analysis

Total RNA from cells or mouse tissues was extracted using TRIzol (Invitrogen, USA). RNA concentration was measured using a spectrophotometer (Nano Drop 1000; Thermo Scientific). RNA samples (1 μg) were reverse transcribed into cDNA using the SuperScript III First-Strand Synthesis System (Invitrogen), following the manufacturer's protocol. The qPCR analysis was performed using a StepOnePlus Real-Time PCR system (Bio-Rad) with the Power SYBR Green PCR Master Mix kit (Applied Biosystems). The thermocycling conditions were as follows: initial denaturation at 95°C for 5 s, followed by 35 cycles of denaturation at 94°C for 15 s, annealing at 55°C for 25 s, and extension at 70°C for 30 s. Primers specific for the M gene of rNDV, PTEN gene, and 18S ribosomal RNA gene were produced by a nucleotide synthesis company (Bioneer, Republic of Korea). Relative expression of mRNA was calculated using the $2^{-\Delta\Delta Ct}$ method.[44] The primer sequences were as follows: rNDV M, forward 5′-AGC TCA TGT GGT TGC AAG GT-3′, reverse 5′-CTG CCT GAA ACT AGG CGG AA-3′; PTEN, forward 5′-CAA GAT GAT GTT TGA AAC TAT-3′, reverse 5′-CCT TTA GCT GGC AGA CCA CAA-3′; 18S (control for mRNA), forward 5′-GTA ACC CGT TGA ACC CCA TT-3′, reverse 5′-CCA TCC AAT CGG TAG TAG CG-3′.

Cell viability assay

To investigate the viability of the selected pancreatic cancer cell lines, the cells were seeded in 96-well plates at a density of 1×10^4 (PANC-1, SNU-213, and AsPC-1) or 5×10^3 (hTERT-HPNE) cells/well, 1 day before virus infection. All the cell lines were infected with rNDV or rNDV-PTEN at an MOI of 1.0. The experiments were replicated in four wells for each group. After incubating for 96 h, the MTT solution (CellTiter 96 AQueous One Solution Cell Proliferation Assay, Promega, USA) was added to each well according to the manufacturer's protocol, and the plates were further incubated at 37°C for 1 h. Thereafter, the absorbance at 490 nm was measured using an

iMark Microplate Reader (catalog #: 1681130EDU, Bio-Rad). The relative cell viability (%) was calculated as described next.

Relative cell viability (%) = (optical density for experimental group/optical density for control group) ×100

PANC-1 cells were seeded in 96-well plates at a density of 1×10^4 cells/well. After 1 day, PANC-1 cells were infected with rNDV or rNDV-PTEN at an MOI of 0.1, 1.0, and 2.5. The experiments were replicated in four wells for each group. After incubating for 12, 24, and 36 h, MTT solution (CellTiter 96 AQueous One Solution Cell Proliferation Assay, Promega) was added to each well according to the manufacturer's protocol, and the plates were further incubated at 37°C for 1 h. Thereafter, the absorbance at 490 nm was measured using an iMark Microplate Reader (catalog #: 1681130EDU, Bio-Rad). The relative cell viability (%) was calculated as described above.

Growth kinetics of rNDV and rNDV-PTEN viruses

The viral growth kinetics of rNDV and rNDV-PTEN was assessed in DF-1 and PANC-1 cells. DF-1 and PANC-1 cells were seeded in a 12-well plate and infected with a rNDV or rNDV-PTEN load of 0.5 MOI. Supernatants were collected at 24, 48, 72, and 96 h post infection. The viral titer was calculated using the method described by Muench and Reed using Vero cells.[45]

Construction of in vivo *LTPA syngeneic mouse model*

Five-week-old female C57BL/6 mice were purchased from Orient Bio (Republic of Korea). LTPA cell is an epithelial cell that was isolated from the pancreas of a 12-month female LT/Sy mouse with adenocarcinoma. For the syngeneic model, LTPA cells (1×10^7 cells/dose) suspended in 100 μL of PBS were mixed with 100 μL of Matrigel (catalog #: 354230, Corning, NY, USA) and injected into the left flank of C57BL/6 mice. Tumor size was measured using a caliper every 2 days, and the volume was calculated as 1/2 × (smallest diameter)^2 × (largest diameter). When the tumor volume reached an average of 100–150 mm^3, the mice were randomly divided into the following groups and i.v. inoculated every 2 days, for a total of five times. The three groups used were as follows: control group (injected with 100 μL of sterile PBS; $n = 5$), rNDV group (injected with 1×10^7 $TCID_{50}$/dose rNDV virus; $n = 5$), and rNDV-PTEN group (injected with 1×10^7 $TCID_{50}$/dose rNDV-PTEN virus; $n = 5$). Blood was collected 1 or 2 days post virotherapy and 3 or 7 days after the fifth virotherapy stop. The blood samples were centrifuged at 1,500 × *g* for 5 min at 4°C, and the supernatant serum was transferred to 1.5-mL microcentrifuge tubes and maintained at −80°C until NDV HN antibody and cytokine analysis using an ELISA. At the end of the experiments, three and two mice per group were sacrificed 3 and 7 days after the fifth virotherapy stop, respectively, and the tumors were collected for immunohistochemical assay.

Quantitation of HN antibody titers and cytokines using ELISA

Blood samples from LTPA syngeneic mice were centrifuged (1,500 × *g* for 15 min), and serum samples, thus obtained, were used for determining the NDV HN antibody titers using VDPro NDV AB ELISA (MEDIAN, Republic of Korea), following the manufacturer's protocol. Then 100 μL of 1:50 diluted serum sample in dilution buffer was added to a 96-well plate, and the plate was allowed to stand for 30 min. The serum sample was discarded, and the plate was washed three times with 300 μL of washing solution. Thereafter, 100 μL of anti-Chicken immunoglobulin (Ig)G HRP conjugate was added to each well, and the plate was incubated for 30 min (25°C ± 1°C). The washing was repeated, followed by the addition of 100 μL of tetramethylbenzidine-hydrogen peroxide as a substrate to each well and incubation (25°C ± 1°C) of the plate for 15 min for color development. Thereafter, 100 μL of stop solution was added to each well, and the absorption at 450 nm was read using an iMark Microplate Reader (catalog #: 1681130EDU, Bio-Rad). The antibody titer in the serum samples was calculated as the absorbance (optical density [OD] 450 nm).

TNFA, IFNA, IL2, and IL6 concentrations in the serum of LTPA syngeneic mice were measured using ELISA (TNFA, ab252352; IFNA, ab208348; IL2, ab100706; and IL6, ab100712; Abcam), following the manufacturer's protocols. The absorbance was measured at 450 nm using an iMark Microplate Reader (catalog #: 1681130EDU, Bio-Rad). All experiments were performed in triplicates.

Construction of in vivo *PANC-1 xenograft mouse model*

Five-week-old female BALB/c nu−/nu− mice were purchased from Orient Bio (Republic of Korea). For the xenograft assay, PANC-1 cells (5×10^6 cells/dose) suspended in sterile PBS were mixed with 100 μL of Matrigel (catalog #: 354230; Corning) and injected into the left flank of mice. Tumor size was measured using a caliper every 2 days, and the volume was calculated as 1/2 × (smallest diameter)^2 × (largest diameter). When the tumor volume reached an average of 100–200 mm^3, the mice were randomly divided into the following groups and i.v. inoculated every 2 days: control group (injected with 100 μL of sterile PBS; $n = 4$), rNDV group (injected with 1×10^7 $TCID_{50}$/dose rNDV viruses; $n = 4$), and rNDV-PTEN group (injected with 1×10^7 $TCID_{50}$/dose rNDV-PTEN viruses; $n = 4$). At the end of the experiments, the mice were sacrificed, and tumors were collected for viral RNA analysis and H&E staining.

Construction of in vivo *PANC-1 orthotopic mouse model*

Five-week-old female BALB/c nu−/nu−mice were purchased from Orient Bio (Republic of Korea). The mice were anesthetized using 250 mg/kg 2,2,2-tribromoethanol (Avertin), and then 5×10^4 PANC-1-Luc2 cells (luciferase sequence included in PANC-1 cells) were injected as follows: an approximately 3-cm incision was made on the left side of the abdomen, the spleen was lifted to expose the pancreas, and 100 μL of the cell suspension was injected using an insulin syringe. The mice were examined using an IVIS every 7 days. After 22 days, the mice were randomly divided into three groups as follows: rNDV (injected with 100 μL of 10^7 $TCID_{50}$/dose every time; i.v.), rNDV-PTEN (injected with 100 μL of 10^7 $TCID_{50}$/dose every time; i.v), and PBS as a negative control ($n = 6$ per group).

In vivo *imaging*

Mice were anesthetized with 2.5% isoflurane, and luciferase imaging was performed 15 min after luciferin injection (100 μL; 30 mg/mL, intraperitoneally [i.p.]) using a Lumina R IVIS (PerkinElmer, USA). The images were captured, and the signals were displayed as radiant efficiency (photons/s/cm^2/steradian [sr] or μW/cm^2). Finally, images of the regions of interest were analyzed using the Living Imaging 4.4 software (Caliper Life Science, USA).

Immunohistochemical assay

Tumor tissue samples were fixed in 4% (w/v) paraformaldehyde and embedded in paraffin. Paraffin sections were deparaffinized, rehydrated according to standard protocols, and stained with H&E. For immunohistochemical analysis, tumor tissues were stained overnight with the primary antibodies, anti-MMP9 (1:500; MA5-15886; Thermo Fisher), anti-PTEN (1:750; 9559S; Cell Signaling Technology), anti-NDV HN (1:750; sc-53562; Santa Cruz Biotechnology, USA), and anti-Ki67 (1:500; MA5-14520; Thermo Fisher), at 4°C. HRP-conjugated anti-rabbit or anti-mouse IgG was added, and the cells were incubated for 60 min at 25°C ± 1°C. The stained sections were developed for 10 s by incubating with 3,3′-diaminobenzidine. The sections were counterstained with hematoxylin and examined under a microscope (Motic, Richmond, BC, Canada) at ×100 magnification.

Immunofluorescence assay

Tumor tissue samples were fixed in 4% (w/v) paraformaldehyde and embedded in paraffin. Paraffin sections were deparaffinized and rehydrated according to standard protocols. For immunofluorescence analysis, tumor tissues were stained overnight with the primary antibodies, anti-CA19-9 (1:500; GTX635389; GeneTex) and anti-NDV HN (1:750; sc-53562; Santa Cruz Biotechnology), at 4°C. The sections were then incubated with rabbit anti-fluorescein isothiocyanate or mouse anti-cyanine 3 (Cy3) antibody (1:500; Jackson ImmunoResearch) for 90 min at room temperature. The sections were counterstained with DAPI and examined under a microscope (Motic, Richmond) at ×100 magnification.

Mouse blood analysis

Blood parameters (GLU, TRIG, total cholesterol [CHOL], AST, ALT, and REA) were analyzed using a Samsung LABGEOPT Biochemistry Test 9 Kit (PR-PT05) with a Samsung LABGEO PT10 analyzer according to the manufacturer's instructions.

Statistical analysis

Statistical analyses were performed using the Prism 8 software (GraphPad Software, La Jolla, CA, USA). Data are presented as mean ± standard error of the mean. Statistical comparisons were performed using the Student's t test. Statistical significance was set at $p < 0.05$.

DATA AND CODE AVAILABILITY

The data generated in this study are publicly available in GEO at GSE183795.

The data generated in this study are available upon request from the corresponding author.

ACKNOWLEDGMENTS

This work was supported by the Technology development Program (S3271268) funded by the Ministry of SMEs and Startups (MSS, Korea).

AUTHOR CONTRIBUTIONS

H.J. initiated and designed the study. S.K., and H.J. wrote the manuscript. B.-K.J. and S.K. performed most of the experiments. J.K., J.H.J., S.K., M.K., and C.-S.K. performed some part of the experiments. B.-K.J. and S.H.J. performed data curation. H.J. supervised the study.

DECLARATION OF INTERESTS

The authors declare no conflict of interest.

SUPPLEMENTAL INFORMATION

Supplemental information can be found online at https://doi.org/10.1016/j.omton.2024.200898.

REFERENCES

1. Siegel, R.L., Miller, K.D., Fuchs, H.E., and Jemal, A. (2022). Cancer statistics, 2022. CA A Cancer J. Clin. *72*, 7–33.
2. Oberstein, P.E., and Olive, K.P. (2013). Pancreatic cancer: why is it so hard to treat? Therap. Adv. Gastroenterol. *6*, 321–337.
3. Conroy, T., Hammel, P., Hebbar, M., Ben Abdelghani, M., Wei, A.C., Raoul, J.L., Choné, L., Francois, E., Artru, P., Biagi, J.J., et al. (2018). FOLFIRINOX or Gemcitabine as Adjuvant Therapy for Pancreatic Cancer. N. Engl. J. Med. *379*, 2395–2406.
4. Yip, H.Y.K., and Papa, A. (2021). Signaling Pathways in Cancer: Therapeutic Targets, Combinatorial Treatments, and New Developments. Cells *10*, 659.
5. Zhang, Z., Zhang, H., Liao, X., and Tsai, H.I. (2023). *KRAS* mutation: The booster of pancreatic ductal adenocarcinoma transformation and progression. Front. Cell Dev. Biol. *11*, 1147676.
6. Pungsrinont, T., Kallenbach, J., and Baniahmad, A. (2021). Role of PI3K-AKT-mTOR Pathway as a Pro-Survival Signaling and Resistance-Mediating Mechanism to Therapy of Prostate Cancer. Int. J. Mol. Sci. *22*, 11088.
7. Fusco, N., Sajjadi, E., Venetis, K., Gaudioso, G., Lopez, G., Corti, C., Rocco, E.G., Criscitiello, C., Malapelle, U., and Invernizzi, M. (2020). *PTEN* Alterations and Their Role in Cancer Management: Are We Making Headway on Precision Medicine? Genes *11*, 719.
8. Masson, G.R., and Williams, R.L. (2020). Structural Mechanisms of PTEN Regulation. Cold Spring Harb. Perspect. Med. *10*, a036152.
9. Georgescu, M.M. (2010). PTEN Tumor Suppressor Network in PI3K-Akt Pathway Control. Genes Cancer *1*, 1170–1177.
10. Maehama, T., and Dixon, J.E. (1998). The tumor suppressor, PTEN/MMAC1, dephosphorylates the lipid second messenger, phosphatidylinositol 3,4,5-trisphosphate. J. Biol. Chem. *273*, 13375–13378.
11. Carnero, A., and Paramio, J.M. (2014). The PTEN/PI3K/AKT Pathway in vivo, Cancer Mouse Models. Front. Oncol. *4*, 252.
12. Tao, J., Xiong, J., Li, T., Yang, Z., Li, X., Li, K., Wu, H., and Wang, C. (2006). Correlation between protein expression of PTEN in human pancreatic cancer and the proliferation, infiltration, metastasis and prognosis. J. Huazhong Univ. Sci. Technol. *26*, 444–447.
13. Alvarez-Garcia, V., Tawil, Y., Wise, H.M., and Leslie, N.R. (2019). Mechanisms of PTEN loss in cancer: It's all about diversity. Semin. Cancer Biol. *59*, 66–79.
14. Ebert, M.P.A., Fei, G., Schandl, L., Mawrin, C., Dietzmann, K., Herrera, P., Friess, H., Gress, T.M., and Malfertheiner, P. (2002). Reduced PTEN expression in the pancreas overexpressing transforming growth factor-beta 1. Br. J. Cancer *86*, 257–262.
15. Si, W., Liu, X., Wei, R., Zhang, Y., Zhao, Y., Cui, L., and Hong, T. (2019). MTA2-mediated inhibition of PTEN leads to pancreatic ductal adenocarcinoma carcinogenicity. Cell Death Dis. *10*, 206.
16. Ma, J., Sawai, H., Matsuo, Y., Ochi, N., Yasuda, A., Takahashi, H., Wakasugi, T., Funahashi, H., Sato, M., and Takeyama, H. (2010). IGF-1 mediates PTEN

suppression and enhances cell invasion and proliferation via activation of the IGF-1/PI3K/Akt signaling pathway in pancreatic cancer cells. J. Surg. Res. *160*, 90–101.

17. Ma, J., Sawai, H., Ochi, N., Matsuo, Y., Xu, D., Yasuda, A., Takahashi, H., Wakasugi, T., and Takeyama, H. (2009). PTEN regulates angiogenesis through PI3K/Akt/VEGF signaling pathway in human pancreatic cancer cells. Mol. Cell. Biochem. *331*, 161–171.
18. Ying, H., Elpek, K.G., Vinjamoori, A., Zimmerman, S.M., Chu, G.C., Yan, H., Fletcher-Sananikone, E., Zhang, H., Liu, Y., Wang, W., et al. (2011). *PTEN* is a major tumor suppressor in pancreatic ductal adenocarcinoma and regulates an NF-kappaB-cytokine network. Cancer Discov. *1*, 158–169.
19. Rascio, F., Spadaccino, F., Rocchetti, M.T., Castellano, G., Stallone, G., Netti, G.S., and Ranieri, E. (2021). The Pathogenic Role of PI3K/AKT Pathway in Cancer Onset and Drug Resistance: An Updated Review. Cancers *13*, 3949.
20. Faghihkhorasani, A., Dalvand, A., Derafsh, E., Tavakoli, F., Younis, N.K., Yasamineh, S., Gholizadeh, O., and Shokri, P. (2023). The role of oncolytic virotherapy and viral oncogenes in the cancer stem cells: a review of virus in cancer stem cells. Cancer Cell Int. *23*, 250.
21. Muthukutty, P., and Yoo, S.Y. (2023). Oncolytic Virus Engineering and Utilizations: Cancer Immunotherapy Perspective. Viruses *15*, 1645.
22. Burman, B., Pesci, G., and Zamarin, D. (2020). Newcastle Disease Virus at the Forefront of Cancer Immunotherapy. Cancers *12*, 3552.
23. Fournier, P., and Schirrmacher, V. (2013). Oncolytic Newcastle Disease Virus as Cutting Edge between Tumor and Host. Biology *2*, 936–975.
24. Pathak, U., Pal, R.B., and Malik, N. (2023). The Viral Knock: Ameliorating Cancer Treatment with Oncolytic Newcastle Disease Virus. Life *13*, 1626.
25. Huang, F., Dai, C., Zhang, Y., Zhao, Y., Wang, Y., and Ru, G. (2022). Development of Molecular Mechanisms and Their Application on Oncolytic Newcastle Disease Virus in Cancer Therapy. Front. Mol. Biosci. *9*, 889403.
26. Lu, X.X., Cao, L.Y., Chen, X., Xiao, J., Zou, Y., and Chen, Q. (2016). *PTEN* Inhibits Cell Proliferation, Promotes Cell Apoptosis, and Induces Cell Cycle Arrest via Downregulating the PI3K/AKT/*hTERT* Pathway in Lung Adenocarcinoma A549 Cells. BioMed Res. Int. *2016*, 2476842.
27. Jung, S., Liu, W., Baek, J., Moon, J.W., Ye, B.D., Lee, H.S., Park, S.H., Yang, S.K., Han, B., Liu, J., and Song, K. (2020). Expression Quantitative Trait Loci (eQTL) Mapping in Korean Patients With Crohn's Disease and Identification of Potential Causal Genes Through Integration With Disease Associations. Front. Genet. *11*, 486.
28. Ren, S., Rehman, Z.U., Shi, M., Yang, B., Qu, Y., Yang, X.F., Shao, Q., Meng, C., Yang, Z., Gao, X., et al. (2019). Syncytia generated by hemagglutinin-neuraminidase and fusion proteins of virulent Newcastle disease virus induce complete autophagy by activating AMPK-mTORC1-ULK1 signaling>. Vet. Microbiol. *230*, 283–290.
29. Cummings, S., Alfonso, A., Hughes, E., Kucera, M., Mabey, B., Singh, N., and Eng, C. (2023). Cancer Risk Associated With *PTEN* Pathogenic Variants Identified Using Multigene Hereditary Cancer Panel Testing. JCO Precis. Oncol. *7*, e2200415.
30. Altomare, D.A., and Khaled, A.R. (2012). Homeostasis and the importance for a balance between AKT/mTOR activity and intracellular signaling. Curr. Med. Chem. *19*, 3748–3762.
31. Berger, M.F., and Mardis, E.R. (2018). The emerging clinical relevance of genomics in cancer medicine. Nat. Rev. Clin. Oncol. *15*, 353–365.
32. Klijn, C., Bot, J., Adams, D.J., Reinders, M., Wessels, L., and Jonkers, J. (2010). Identification of networks of co-occurring, tumor-related DNA copy number changes using a genome-wide scoring approach. PLoS Comput. Biol. *6*, e1000631.
33. Ku, J.L., and Park, J.G. (2005). Biology of SNU cell lines. Cancer Res. Treat. *37*, 1–19.
34. Stambolic, V., MacPherson, D., Sas, D., Lin, Y., Snow, B., Jang, Y., Benchimol, S., and Mak, T.W. (2001). Regulation of PTEN transcription by p53. Mol. Cell *8*, 317–325.
35. Cetintas, V.B., and Batada, N.N. (2020). Is there a causal link between PTEN deficient tumors and immunosuppressive tumor microenvironment? J. Transl. Med. *18*, 45.
36. Panwar, V., Singh, A., Bhatt, M., Tonk, R.K., Azizov, S., Raza, A.S., Sengupta, S., Kumar, D., and Garg, M. (2023). Multifaceted role of mTOR (mammalian target of rapamycin) signaling pathway in human health and disease. Signal Transduct. Targeted Ther. *8*, 375.
37. Glaviano, A., Foo, A.S.C., Lam, H.Y., Yap, K.C.H., Jacot, W., Jones, R.H., Eng, H., Nair, M.G., Makvandi, P., Geoerger, B., et al. (2023). PI3K/AKT/mTOR signaling transduction pathway and targeted therapies in cancer. Mol. Cancer *22*, 138.
38. Bu, H., Liu, D., Zhang, G., Chen, L., and Song, Z. (2020). AMPK/mTOR/ULK1 Axis-Mediated Pathway Participates in Apoptosis and Autophagy Induction by Oridonin in Colon Cancer DLD-1 Cells. OncoTargets Ther. *13*, 8533–8545.
39. Marquez, R.T., and Xu, L. (2012). Bcl-2:Beclin 1 complex: multiple, mechanisms regulating autophagy/apoptosis toggle switch. Am. J. Cancer Res. *2*, 214–221.
40. Freeman, A.I., Zakay-Rones, Z., Gomori, J.M., Linetsky, E., Rasooly, L., Greenbaum, E., Rozenman-Yair, S., Panet, A., Libson, E., Irving, C.S., et al. (2006). Phase I/II trial of intravenous NDV-HUJ oncolytic virus in recurrent glioblastoma multiforme. Mol. Ther. *13*, 221–228.
41. Csatary, L.K., Gosztonyi, G., Szeberenyi, J., Fabian, Z., Liszka, V., Bodey, B., and Csatary, C.M. (2004). MTH-68/H oncolytic viral treatment in human high-grade gliomas. J. Neuro Oncol. *67*, 83–93.
42. Chen, Y., Zhu, S., Liao, T., Wang, C., Han, J., Yang, Z., Lu, X., Hu, Z., Hu, J., Wang, X., et al. (2024). The HN protein of Newcastle disease virus induces cell apoptosis through the induction of lysosomal membrane permeabilization. PLoS Pathog. *20*, e1011981.
43. Jang, S.H., Jung, B.K., An, Y.H., and Jang, H. (2022). The phosphatase and tensin homolog gene inserted between NP and P gene of recombinant New castle disease virus oncolytic effect test to glioblastoma cell and xenograft mouse model. Virol. J. *19*, 21.
44. Livak, K.J., and Schmittgen, T.D. (2001). Analysis of relative gene expression data using real-time quantitative PCR and the 2(-Delta Delta C(T)) Method. Methods *25*, 402–408.
45. Lei, C., Yang, J., Hu, J., and Sun, X. (2021). On the Calculation of $TCID_{50}$ for Quantitation of Virus Infectivity. Virol. Sin. *36*, 141–144.